Optical Materials 36 (2014) 1631–1635

Contents lists available at ScienceDirect

Optical Materials

journal homepage: www.elsevier.com/locate/optmat

Synthesis and spectroscopic properties of multiferroic β′-$Tb_2(MoO_4)_3$

V.V. Atuchin [a], A.S. Aleksandrovsky [b], O.D. Chimitova [c], A.S. Krylov [d], M.S. Molokeev [e], B.G. Bazarov [c], J.G. Bazarova [c], Zhiguo Xia [f,*]

[a] Laboratory of Optical Materials and Structures, Institute of Semiconductor Physics, SB RAS, Novosibirsk 630090, Russia
[b] Laboratory of Coherent Optics, Kirensky Institute of Physics, SB RAS, Akademgorodok, Krasnoyarsk 660036, Russia
[c] Laboratory of Oxide Systems, Baikal Institute of Nature Management, SB RAS, Ulan-Ude 670047, Russia
[d] Laboratory of Molecular Spectroscopy, Kirensky Institute of Physics, SB RAS, Krasnoyarsk 660036, Russia
[e] Laboratory of Crystal Physics, Kirensky Institute of Physics, SB RAS, Krasnoyarsk 660036, Russia
[f] School of Materials Sciences and Technology, China University of Geosciences, Beijing 100083, China

ARTICLE INFO

Article history:
Available online 4 January 2014

Keywords:
Terbium molybdate
Raman spectrum
Optical properties

ABSTRACT

Orthorhombic terbium molybdate, β′-$Tb_2(MoO_4)_3$, microcrystals have been fabricated by solid state synthesis at $T = 750–1270$ K for $t = 290$ h. The crystal structure β′-$Tb_2(MoO_4)_3$ has been refined by Rietveld method in space group *Pba*2 with cell parameters of $a = 10.35387(6)$, $b = 10.38413(6)$ and $c = 10.65695(7)$ Å ($R_B = 1.83\%$). About 40 narrow Raman lines have been observed in the Raman spectrum recorded for the β′-$Tb_2(MoO_4)_3$ powder sample. The luminescence spectrum of β′-$Tb_2(MoO_4)_3$ has been measured under the excitation at 355 nm, and the intensive photoluminescence band at 540–550 nm has been found.

1. Introduction

Molybdate crystals have become of considerable interest for detailed evaluation because of their valuable structural, luminescent and spectroscopic properties promising for practical applications in laser and photonic technologies [1–5]. The molybdates containing rare-earth elements are of special attention because of their specific spectroscopic properties [4,6–16]. As a rule, in the molybdates the rare-earth ions are in low symmetry positions, and this is a key factor for the creation of effective luminescent media. In the development of new optical materials, however, it is reasonable to explore the long-discovered but less studied complex molybdate crystals because, as a rule, only fragmentary spectroscopic information can be found in the literature, and the crystal's potentials are unclear in many aspects.

Terbium molybdate, $Tb_2(MoO_4)_3$, belongs to a wide family of $Ln_2(MoO_4)_3$ compounds which intriguing physical properties have been under investigation for many years [17]. Generally, the molybdates possess a sequence of the phase transitions with a temperature variation, and the β and β′ polymorph modifications are noncentrosymmetric [17–21]. As it was shown, orthorhombic phase β′-$Tb_2(MoO_4)_3$, space group *Pba*2, appears at the temperatures below 433 K [20,21]. The crystal structure of β′-$Tb_2(MoO_4)_3$ is depicted in Fig. 1. The structure can be considered as a framework formed by MoO_4 tetrahedrons and TbO_7 polyhedrons linked by corners. The unit cell is large: it includes 68 atoms and possesses as high cell volume as $V = 1146.41$ Å^3 [21]. This ferroelectric modification possesses interesting acoustic, optical and magnetic properties [22–28]. In several experiments, the β′-$Tb_2(MoO_4)_3$ optical quality single crystals were prepared by Czochralski growth due to a low level of mechanical tensions induced by the β↔β′ phase transition on cooling, and anisotropic material constants of β′-$Tb_2(MoO_4)_3$ were defined [20,22,24,26,28–33].

The spectroscopic properties of β′-$Tb_2(MoO_4)_3$ were evaluated in several studies [28,30–32,34,35]. The β′-$Tb_2(MoO_4)_3$ crystals are transparent over the range of ~340–1750 nm, and the optical band gap was estimated to be $E_g \sim 3.76$ eV [28,30–32]. The strong absorption bands related to Tb^{3+} ions were observed in the infrared spectral range at 1750–2000, ~2250 and 2800–3150 nm for the pale-green orthorhombic β′-$Tb_2(MoO_4)_3$ crystal [30]. In the visible range, the sharp absorption line was found at ~485 nm [30–32]. The photoluminescence spectra of $Tb_2(MoO_4)_3$ crystals were recorded in Ref. [18], and the bands were found at 490, 540, 580 and 615 nm. It should be pointed, however, that the phase composition of the crystal was not clear, and the luminescence spectra were recorded at a low resolution. $Tb_2(MoO_4)_3$ Raman spectra were earlier measured in Refs. [23,32,34,35], and in the cases the samples' phase composition was not verified. Therefore, the present study is meant to produce the evaluation of structural and spectroscopic properties of the β′-$Tb_2(MoO_4)_3$ molybdate with

* Corresponding author. Address: School of Materials Sciences and Technology, China University of Geosciences, No. 29 Xueyuan Road, Beijing 100083, China. Tel.: +86 10 8233 2247; fax: +86 10 8232 2974.
E-mail address: xiazg@cugb.edu.cn (Z. Xia).

0925-3467/$ - see front matter © 2013 Elsevier B.V. All rights reserved.
http://dx.doi.org/10.1016/j.optmat.2013.12.008

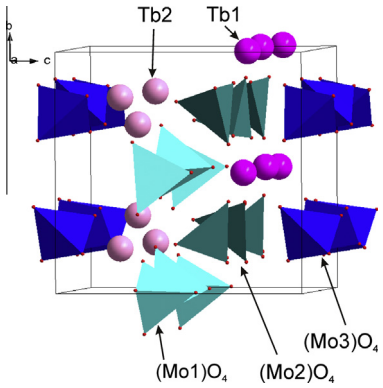

Fig. 1. Crystal structure of β′-$Tb_2(MoO_4)_3$. The unit cell is outlined.

Table 1
The main parameters of processing and refinement.

Space group	*Pba2*
a (Å)	10.35387(6)
b (Å)	10.38413(6)
c (Å)	10.65695(7)
V (Å^3)	1145.79(1)
2θ-interval range (°)	5–140
Number of reflexions	1160
Number of refinement parameters	113
R_{wp} (%)	1.83
R_p (%)	1.35
R_B (%)	0.73
χ^2	1.70

the emphasis on the photoluminescence characteristics of this promising host.

2. Experimental methods and data processing

The powder polycrystalline sample of β′-$Tb_2(MoO_4)_3$ was prepared using the solid state reaction in a platinum crucible. Analytically pure Tb_4O_7 (Aldrich, 99.9%) and MoO_3 (Alfa Aesar, 99.95%) were used as starting materials. Before synthesis, to remove the admixture of residual water occasionally captured from the air, the Tb_4O_7 and MoO_3 oxides were being annealed at $T = 1173$ K and 723 K, respectively, for 10 h. Then, these pre-heated powders were weighed in stoichiometric amounts, mixed and homogenized in an agate mortar. The synthesis reaction was carried out in two steps: the first annealing at 753 K and the second one at 873 K for 30 and 200 h, respectively. This first step was followed by a careful grinding and homogenization of the agglomerate in an agate mortar and firing at 923 K and 1273 K for 40 and 20 h, respectively. Such route of the multi-step synthesis is optimal for molybdates because of the danger of MoO_3 loss due to a relatively high volatility of this oxide in the air [36–38]. After cooling to room temperature, the final product was formed.

The X-ray powder diffraction of $Tb_2(MoO_4)_3$ was measured at room temperature (25 °C) with a Bruker D8 ADVANCE powder diffractometer in the Bragg–Brentano geometry and linear VANTEC detector. The operating parameters were as follows: Cu Kα tube voltage 40 kV, tube current 40 mA radiation, step size 0.016°, and counting time 10 s per step. The beam was controlled by the 0.6 mm fixed divergence slit, 6 mm receiving VANTEC slit and Soller slits. The data were collected over the range of 2θ: 5–140°. The peak positions were determined with EVA program, available in the PC software package DIFFRAC-PLUS supplied from Bruker. The TOPAS 4.2 [39] program was used for the Rietveld refinement.

The unpolarized Raman spectra were collected in a backscattering geometry using a triple monochromator Horiba Jobin Yvon T64000 Raman spectrometer operating in a double subtractive mode, then detected by an LN-cooled charge-coupled device. The spectral resolution for the recorded Stokes side of the Raman spectra was set to ~2 cm^{-1} (this resolution was achieved by using gratings with 1800 grooves/mm and 100 mm slits). The microscope system based on Olympus BX41 microscope with a 50× objective lens $f = 0.8$ mm with NA = 0.75 numerical aperture provides a focal spot diameter of about 5 μm on the sample. The single-mode argon line of 514.5 nm from a Spectra-Physics Stabilite 2017 Ar^+ laser of 5 mW on the sample was used as the excitation light source. The laser light intensity was adjusted to avoid the sample's heating. The spectral lines' wavenumber position and width were obtained by the least square fitting of the experimental data to Lorentzian equation [40]:

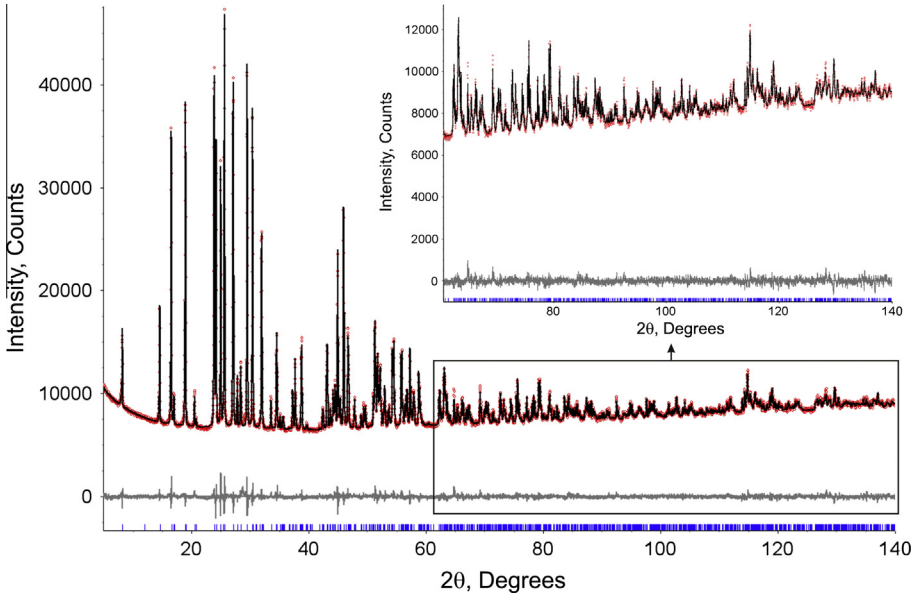

Fig. 2. Rietveld difference plot of β′-$Tb_2(MoO_4)_3$ at room temperature.

Table 2
The atom coordinates and isotropic thermal parameters (B_{iso}) of the β′-$Tb_2(MoO_4)_3$ structure.

Atom	x	y	z	B_{iso}
Tb1	0.1870 (2)	0.4962 (6)	0.7373 (4)	0.34 (7)
Tb2	0.4939 (5)	0.31230 (19)	0.2637 (4)	0.43 (7)
Mo1	0.2051 (3)	0.4895 (6)	0.3563 (5)	0.24 (8)
Mo2	0.0035 (7)	0.2071 (3)	0.6423 (5)	0.44 (8)
Mo3	0.2423 (6)	0.2414 (6)	0	0.25 (6)
O1	0.1942 (19)	0.497 (4)	0.524 (3)	0.61 (13)
O2	0.481 (3)	0.2949 (18)	0.490 (3)	0.61 (13)
O3	0.133 (2)	0.010 (4)	0.305 (2)	0.61 (13)
O4	0.496 (5)	0.118 (2)	0.703 (2)	0.61 (13)
O5	0.160 (3)	0.145 (3)	0.674 (3)	0.61 (13)
O6	0.161 (2)	0.324 (3)	0.310 (3)	0.61 (13)
O7	0.401 (2)	0.370 (3)	0.711 (3)	0.61 (13)
O8	0.389 (2)	0.124 (3)	0.298 (3)	0.61 (13)
O9	0.139 (3)	0.162 (3)	0.090 (3)	0.61 (13)
O10	0.300 (3)	0.129 (3)	0.901 (3)	0.61 (13)
O11	0.352 (3)	0.315 (3)	0.110 (3)	0.61 (13)
O12	0.175 (3)	0.355 (3)	0.887 (4)	0.61 (13)

Table 3
The main interatomic distances in structure β′-$Tb_2(MoO_4)_3$ at room temperature.

Bond	Length (Å)	Bond	Length (Å)
Tb1—O1	2.27 (3)	Mo1—O1	1.80 (3)
Tb1—$O4^{i}$	2.31 (5)	Mo1—$O3^{i}$	1.78 (2)
Tb1—$O4^{ii}$	2.33 (5)	Mo1—O6	1.85 (3)
Tb1—$O5^{i}$	2.31 (3)	Mo1—$O8^{i}$	1.82 (3)
Tb1—O7	2.59 (3)	Mo2—$O2^{ii}$	1.64 (3)
Tb1—$O10^{i}$	2.23 (3)	Mo2—$O4^{ii}$	1.93 (2)
Tb1—O12	2.17 (4)	Mo2—O5	1.78 (3)
Tb2—O2	2.42 (3)	Mo2—$O7^{ii}$	1.52 (3)
Tb2—$O3^{i}$	2.48 (3)	Mo3—O9	1.66 (3)
Tb2—$O3^{iii}$	2.38 (3)	Mo3—$O10^{iv}$	1.68 (3)
Tb2—$O6^{iii}$	2.29 (3)	Mo3—O11	1.80 (3)
Tb2—O8	2.26 (3)	Mo3—$O12^{iv}$	1.83 (4)
Tb2—$O9^{iii}$	2.40 (3)	O4—$O4^{v}$	2.46 (3)
Tb2—O11	2.20 (3)		

Symmetry operators: (i) $-x+1/2$, $y+1/2$, z; (ii) $x-1/2$, $-y+1/2$, z; (iii) $x+1/2$, $-y+1/2$, z; (iv) x, y, $z-1$; (v) $-x+1$, $-y$, z.

$$I_L = \frac{A}{1+\left(\frac{x-\omega}{\Gamma}\right)^2}$$

where A – amplitude, ω – wavenumber, Γ – full width at half height, and x – actual coordinate (wavenumber).

Luminescence spectra were taken using LOMO DFS-24 spectrophotometer at the resolution of 3 cm^{-1}. LaserCompact LCS-DTL-374QT DPSS laser generating 20 mW power at 355 nm was used as an excitation source.

3. Results and discussion

The final powder product prepared by the synthesis route is white with the light pearl-lemon tint typical of terbium oxides. It should be pointed that the powder color is evidently different from the pale-green color earlier shown for the β′-$Tb_2(MoO_4)_3$ crystal grown in N_2 atmosphere [28]. For this reason, the presence of a noticeable oxygen vacancies quantity in the β′-$Tb_2(MoO_4)_3$ crystal may be supposed. The phase purity of the β′-$Tb_2(MoO_4)_3$ powder sample was verified by XRD measurements and structure refinement. The recorded XRD pattern is shown in Fig. 2. Earlier, it was found that $Tb_2(MoO_4)_3$ has two phases: (1) tetragonal phase $P\text{-}42_1m$ at the temperatures higher than 432 K [20]; (2) orthorhombic phase $Pba2$ at temperatures lower than 433 K [20,21]. As the powder pattern was measured at room temperature, the cell parameters and atom coordinates of the orthorhombic phase were used as a starting model in the structure refinement. The refinement was stable and it gives low R-factors (Table 1). All atoms were refined with isotropic thermal parameters. All oxygen atoms were refined to have the same thermal parameter. The final atom coordinates and thermal parameters are shown in Table 2. All bond lengths obtained by refinement are presented in Table 3. The values are in good relation to those earlier reported for the β′-$Tb_2(MoO_4)_3$ phase [20,21].

The Raman spectrum recorded from β′-$Tb_2(MoO_4)_3$ is shown in Fig. 3a. The spectrum decomposition is shown in Fig. 3b–d, and the fitted parameters are presented in Table 4. About 40 narrow Raman lines were revealed by the experimental spectrum fitting. The wide

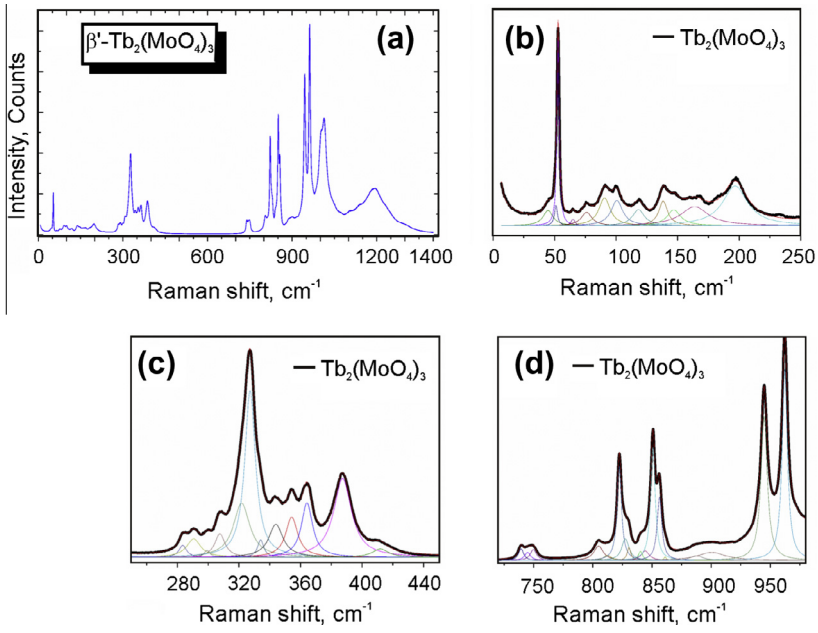

Fig. 3. (a) Survey β′-$Tb_2(MoO_4)_3$ Raman spectrum and spectrum decomposition over (b) low, (c) middle and (d) high wavenumber ranges. Experimental and calculated envelope curves are shown by black and red, respectively. (For interpretation of the references to color in this figure legend, the reader is referred to the web version of this article.)

Table 4
The relative magnitude (I), wavenumber and full width at half maximum (FWHM) of the Raman lines measured from β′-$Tb_2(MoO_4)_3$. The parameters obtained in the present study are marked with asterisk.

Number	A^*	[32]	[34]	ω (wavenumber)* (cm^{-1})	Γ (FWHM)* (cm^{-1})
1	77			44.7	9.7
2	104			51.2	3.0
3	957	53		53.0	2.2
4	33			65.1	3.9
5	68			76.0	10.5
6	141			90.7	11.2
7	128			100.6	11.5
8	81		119	118.2	11.8
9	124		138	138.2	8.8
10	80			146.9	13.4
11	97		164	163.8	26.9
12	201		196	196.7	24.6
13	114			283.4	5.9
14	176		290	290.6	11.1
15	66			299.3	4.5
16	225		307	307.6	8.0
17	514			321.7	12.9
18	1587	327	328	327.3	8.4
19	167			334.1	4.8
20	313		344	344.0	11.3
21	382			354.3	9.5
22	518	364	365	364.2	8.9
23	749	386	390	387.4	14.0
24	79		421	411.9	12.5
25	260			739.3	5.2
26	177		740	744.9	6.1
27	241	750	750	749.7	6.3
28	319	806	807	804.9	9.6
29	113			812.4	7.8
30	2110		822	822.4	4.5
31	483			827.5	7.4
32	285	830	831	830.6	3.7
33	203			840.3	4.3
34	209			844.3	8.2
35	2533	850	850	850.8	4.7
36	1409	858	856	856.4	4.7
37	74			861.2	2.6
38	103		888	887.7	13.4
39	178			900.5	28.6
40	3217	944	944	944.8	6.5
41	4268	962	961	962.2	5.5

bands appeared above 1000 cm^{-1} were related to the luminescence of Tb^{3+} ions. The Raman spectrum of β′-$Tb_2(MoO_4)_3$ can be divided into two parts with a wide empty gap of 400–730 cm^{-1} that is commonly observed in molybdates with MoO_4 tetrahedrons [4,6,9,10,13,14,16,41,42]. In the range of stretched vibrations of MoO_n polyhedra (700–1000 cm^{-1}), a lot of lines were observed because of the presence of several independent and distorted MoO_4 tetrahedrons. The narrowest (FWHM is 5.5 cm^{-1}) and intensive line is detected at 962.2 cm^{-1}. This line can be considered as an analog of the Mo=O stretch line of the α-MoO_3 crystal (995 cm^{-1}) [38]. The total suite of Raman lines found in β′-$Tb_2(MoO_4)_3$ is shown in Table 4 in comparison with the earlier measurements of this molybdate. As it is evident, all earlier detected lines are found in our experiment.

The photoluminescence spectrum of powder β′-$Tb_2(MoO_4)_3$ is presented in Fig. 4 together with the reference spectra of monoclinic multidomain elpasolite Rb_2KTbF_6, space group $P2_1/n$, and single crystalline sample of terbium gallium garnet $Tb_3Ga_5O_{12}$ (TGG), space group Ia-$3d$, the latter being well known as a commercial material for Faraday rotators and isolators. The powder samples of terbium molybdate and the Rb_2KTbF_6 elpasolite were of approximately the same dimensions, while the terbium garnet sample was of much greater dimensions. Generally, all three crystals reveal the characteristic Tb^{3+} luminescence bands and lines. However, the wavelengths and relative intensities of the sharp lines are different and dependent on the environment of Tb^{3+} ions in the crystal lattice. The luminescence in TGG was of the smallest intensity, while, in elpasolite and molybdate, it was of the same order of magnitude. The luminescence of our powder sample strongly differs from that of both single crystalline and powder samples of the orthorhombic β′-$Tb_2(MoO_4)_3$ investigated by Peng et al. [32]. The peak in the region of 540 nm is much narrower in our sample and has an evident vibronic replica. The environment of Tb^{3+} ion in garnets is a parity-breaking one, and the luminescence spectrum is influenced by the crystal field induced transitions with relatively large oscillator strengths as well as vibronic ones. The environment of Tb^{3+} ion in the elpasolite structure is non-parity-breaking, but the central symmetry can be broken at the domain boundaries as investigated in a closely related case of monoclinic holmium elpasolite [43]. Based on these considerations, we can deduce that concentration quenching of Tb luminescence in the molybdate under study is considerably weaker than in the garnet sample and it is of the same order as in elpasolite with its lower energy phonon spectrum and sequent weaker radiation-free relaxation. The Tb^{3+} ions in β′-$Tb_2(MoO_4)_3$ under study occupy two nonequivalent positions. The local environment of Tb^{3+} ions in both positions is a septavertex polyhedron with a lack of inversion

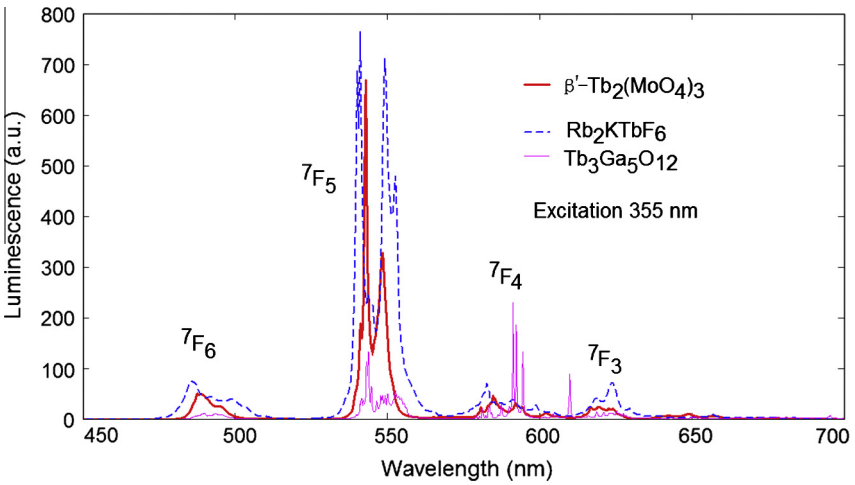

Fig. 4. Photoluminescence spectrum of powder β′-$Tb_2(MoO_4)_3$, monoclinic multidomain elpasolite Rb_2KTbF_6 and a single crystalline sample of terbium gallium garnet $Tb_3Ga_5O_{12}$ (TGG), Terminating levels of transitions from the $^5D_4$ level of Tb^{3+} ion are indicated.

center that produces noticeable crystal field induced oscillator strengths at the luminescing transitions and favors a more efficient emission.

4. Conclusions

The structural quality of polycrystalline β′-$Tb_2(MoO_4)_3$ provides the detailed observation of spectroscopic parameters of this ferroelectric molybdate. A lot of narrow lines are found in Raman spectrum. The spectrum of β′-$Tb_2(MoO_4)_3$ luminescence is found to be of noticeably different shapes as compared to that of terbium gallium garnet. The concentration quenching in β′-$Tb_2(MoO_4)_3$ is suspected to be of rather a modest rate. The information can be used as a firm basis for the exploration of doped and complex luminescent molybdates.

Acknowledgments

This study was partly supported by SB RAS under Projects 28.13 and 24.31, and by the PSB RAS Project No. 3.9.5b, and RFBR Projects 11-08-00681a and 11-03-00867a.

References

[1] T.T. Basiev, A.A. Sobol, Yu.K. Voronko, P.G. Zverev, Opt. Mater. 15 (2000) 205–216.
[2] A. Brenier, D. Jaque, A. Majchrowski, Opt. Mater. 28 (2006) 310–323.
[3] Z.G. Xia, D.M. Chen, J. Am. Ceram. Soc. 93 (2010) 1397–1401.
[4] M. Maczka, A.G. Souza Filho, W. Paraguassu, P.T.C. Freire, J. Mendes Filho, J. Hanuza, Prog. Mater. Sci. 57 (2012) 1335–1381.
[5] C.S. Lim, V.V. Atuchin, Proc. SPIE 8771 (2013) 877110.
[6] A.A. Kaminskii, A.V. Butashin, H.-J. Eichler, D. Grebe, R. Macdonald, K. Ueda, H. Nishioka, W. Odajima, M. Tateno, J. Song, M. Musha, S.N. Bagaev, A.A. Pavlyuk, Opt. Mater. 7 (1997) 59–73.
[7] P. Becker, L. Bohatý, H. Rhee, H.J. Eichler, J. Hanuza, A.A. Kaminskii, Laser Phys. Lett. 5 (2008) 114–121.
[8] Z.G. Xia, J.F. Sun, H.Y. Du, D.M. Chen, J.Y. Sun, J. Mater. Sci. 45 (2010) 1553–1559.
[9] H. Fuks, S.M. Kaczmarek, G. Leniec, L. Macalik, B. Macalik, J. Hanuza, Opt. Mater. 32 (2010) 1560–1567.
[10] V.V. Atuchin, O.D. Chimitova, T.A. Gavrilova, M.S. Molokeev, Sung-Jin Kim, N.V. Surovtsev, B.G. Bazarov, J. Cryst. Growth 318 (2011) 683–686.
[11] G. Benoît, J. Véronique, A. Arnaud, G. Alain, Solid State Sci. 13 (2011) 460–467.
[12] Z.G. Xia, S. Jin, J.Y. Sun, H. Y Du, P. Du, L.B. Liao, J. Nanosci. Nanotechnol. 11 (2011) 9612–9620.
[13] M. Mączka, M. Ptak, C. Luz-Lima, P.T.C. Freire, W. Paraguassu, S. Guerini, J. Hanuza, J. Solid State Chem. 184 (2011) 2812–2817.
[14] V.V. Atuchin, V.G. Grossman, S.V. Adichtchev, N.V. Surovtsev, T.A. Gavrilova, B.G. Bazarov, Opt. Mater. 34 (2012) 812–816.
[15] J.F. Tang, Y.J. Chen, Y.F. Lin, X.H. Gong, J.H. Huang, Z.D. Luo, Y.D. Huang, Opt. Mater. Express 2 (2012) 1064–1075.
[16] V.V. Atuchin, O.D. Chimitova, S.V. Adichtchev, B.G. Bazarov, T.A. Gavrilova, M.S. Molokeev, N.V. Surovtsev, Zh.G. Bazarova, Mater. Lett. 106 (2013) 26–29.
[17] H.J. Borchardt, P.E. Bierstedt, J. Appl. Phys. 18 (1967) 2057–2060.
[18] E.T. Keve, S.C. Abrahams, K. Nassau, A.M. Glass, Solid State Commun. 8 (1970) 1517–1520.
[19] E.T. Keve, S.C. Abrahams, J.L. Berstein, J. Chem. Phys. 54 (1971) 3185–3194.
[20] S.C. Abrahams, C. Svensson, J.L. Bernstein, J. Chem. Phys. 72 (1980) 4278–4285.
[21] C. Svensson, S.C. Abrahams, J.L. Bernstein, J. Chem. Phys. 71 (1979) 5191–5195.
[22] J.M. Courdille, R. Deroche, J. Dumas, J. Phys. 36 (1975) 891–895.
[23] P.A. Fleury, K.B. Lyons, R.S. Katiyar, Phys. Rev. B 26 (1982) 6397–6407.
[24] R.C. Miller, W.A. Nordland, K. Nassau, Ferroelectrics 2 (1971) 97–99.
[25] R. Bonneville, F. Auzel, J. Chem. Phys. 67 (1977) 4597–4602.
[26] B.K. Ponomarev, S.A. Ivanov, B.S. Red'kin, V.N. Kurlov, J. Appl. Phys. 75 (1994) 8004–8007.
[27] B.K. Ponomarev, Ferroelectrics 280 (2002) 95–117.
[28] B.K. Ponomarev, B.S. Red'kin, A.G.M. Jansen, P. Wyder, H. Wiegelmann, E. Steep, Phys. Solid State 50 (2008) 1495–1501.
[29] B.A. Strukov, S.A. Taraskin, I.V. Shnaidshtein, S.V. Pavlov, A. Onodera, H. Haga, B.K. Red'kin, Cryst. Rep. 42 (1997) 990–992.
[30] M. Xu, Y.G. Yu, H.J. Zhang, J.Y. Wang, J. Rare Earths 27 (2009) 192–195.
[31] G.P. Cai, J.Y. Wang, H.J. Zhang, Cryst. Res. Technol. 44 (2009) 1001–1004.
[32] S. Peng, W. Cai, X.F. Wang, Y. Kan, F.Z. Huang, M. Xu, H.J. Zhang, J.Y. Wang, X.M. Lu, J.S. Zhu, Ferroelectrics 410 (2011) 69–74.
[33] M. Xu, W.L. Gao, H.J. Zhang, X.F. Cheng, X.G. Xu, J.Y. Wang, R.I. Boughton, J. Alloys Compd. 509 (2011) 8455–8459.
[34] A. Jayaraman, S.K. Sharma, Z. Wang, S.Y. Wang, L.C. Ming, M.H. Manghnani, J. Phys. Chem. Solids 54 (1993) 827–833.
[35] E. Islam, A. Sakai, A. Onodera, B.A. Strukov, J. Korean Phys. Soc. 32 (1998) 8506–8508.
[36] B.G. Bazarov, R.F. Klevtsova, O.D. Chimitova, L.A. Glinskaya, K.N. Fedorov, Y.L. Tushinova, Z.G. Bazarova, Russ. J. Inorg. Chem. 51 (2006) 800–804.
[37] O.D. Chimitova, B.G. Bazarov, K.N. Fedorov, Z.G. Bazarova, Russ. J. Appl. Chem. 81 (2008) 2043–2044.
[38] V.V. Atuchin, T.A. Gavrilova, T.I. Grigorieva, N.V. Kuratieva, K.A. Okotrub, N.V. Pervulhina, N.V. Surovtsev, J. Cryst. Growth 318 (2011) 987–990.
[39] Bruker AXS TOPAS V4: General profile and structure analysis software for powder diffraction data – User's Manual, Bruker AXS, Karlsruhe, Germany, 2008.
[40] Peter A. Jansson, Deconvolution with Applications in Spectroscopy, Academic Press, 1984.
[41] B.A. Kolesov, L.P. Kozeeva, J. Struct. Chem. 34 (1993) 534–539.
[42] A. Jayaraman, S.K. Sharma, S.Y. Wang, S.R. Shieh, L.C. Ming, S.-W. Cheong, Pramana J. Phys. 47 (1996) 151–161.
[43] A.S. Aleksandrovsky, A.S. Krylov, A.V. Malakhovskii, V.N. Voronov, J. Lumin. 132 (2012) 690–692.